
SWITCHCRAFT: Programmatic Design of State-Switching Proteins

Bowen Jing^{1†}, Mihir Bafna^{1†}, Adam Klivans², Bonnie Berger¹

¹Massachusetts Institute of Technology ²University of Texas at Austin

[†]Equal contribution. Correspondence to {bjing, mihirb14}@mit.edu

Abstract

Complex multistate functional mechanisms are observed ubiquitously in natural proteins, yet the path towards systematic *de novo* rational design of such mechanisms remains unclear, despite significant advancements in protein language models and structure diffusion models. We introduce SWITCHCRAFT, a versatile and programmatic framework for state-switching proteins based on backpropagation through compositional design constraints parameterized by structure prediction models. Our *in silico* evaluations demonstrate success on a wide range of state-switching design specifications, from allosteric regulation of functional motifs to discrimination of bound ligand identities. Notably, one design exhibits a 3.8 Å conformational change upon oxygenation of heme, mimicking mechanisms of cooperativity in hemoglobin. These results position SWITCHCRAFT at the inception of a powerful paradigm for higher-order functional protein design.

1 Introduction

Generative models have driven unprecedented advancements in protein design. Protein language models (PLMs), trained on datasets of existing functional proteins, can generate novel sequences with similar or improved properties (Madani et al., 2023; Hayes et al., 2025; Ruffolo et al., 2025; Lambert et al., 2025); while structure generation models have become widely used for the design of *de novo* binders and scaffolding of simple enzymatic sites (Watson et al., 2023; Krishna et al., 2024; Lauko et al., 2025; Ahern et al., 2025). However, many natural proteins involve multiple structural states and modulation of state populations by effector molecules, as observed in allosteric regulation, signal transduction, motor proteins, and multistep enzymes (Grant et al., 2010). Yet, existing generative modeling frameworks do not provide a means for the rational design of these types of mechanisms. While PLMs can recapitulate a wide range of complex existing functions, they cannot be prompted to design new functions based on fine-grained specifications. On the other hand, structure generators are necessarily limited to designing static structures and thus relatively simple functions.

To broadly enable the development of multistate proteins with complex functions, we develop SWITCHCRAFT, a programmatic framework for generating proteins that activate, deactivate, or switch between functional states based on the presence of a ligand effector. Our method builds upon techniques for single-state protein design that use backpropagation on structure prediction models, which have been highly effective at designing protein and small molecule binders (Pacesa et al., 2025; Cho et al., 2025). In our framework, a generic protein design problem is specified via an arbitrary number of *states*, each of which is described via an arbitrary number of *constraints* that can be evaluated using the output of the structure prediction model. As such, our method can in principle be applied to any functions that can be described using a set of structural properties partitioned across multiple states. In this work, we focus on constraints based on binding with a ligand or scaffolding of backbone motifs, which encompasses a wide range of functions targeted in the current protein design literature (Wang et al., 2022; Watson et al., 2023; Pacesa et al., 2025).

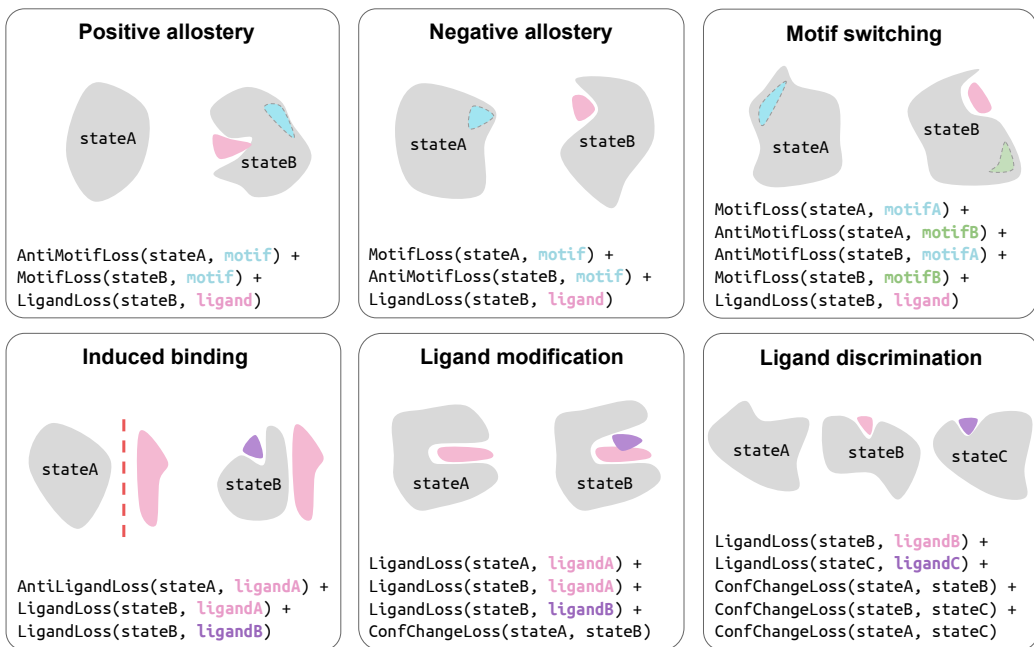


Figure 1: Versatile and programmatic multistate design capabilities enabled by SWITCHCRAFT. All specifications also include a `ContactLoss` term for each distinct protein state.

Our experiments explore several different variations on this theme, as illustrated in Figure 1. For the simplest case of single ligands activating (positive allostery) or deactivating (negative allostery) a structural motif, we systematically use a diverse set of ligands, including small molecules, metal ions, and DNA, to modulate 11 of the 24 motifs from the well-known RFDiffusion motif scaffolding benchmark (Wang et al., 2022; Watson et al., 2023). We then demonstrate individual designs for more complex design specifications: proteins that switch between two motifs with a ligand effector (motif switching); that bind a target protein only in the presence of a ligand (induced binding); that exhibit a large conformational shift upon change to a bound ligand—specifically, oxygenation of a bound heme (ligand modification); and that switch between three distinct conformations depending on which of two ligands is bound (ligand discrimination). Remarkably, we obtain these designs with relatively little tuning and filtering, even for highly compositional design specifications.

2 Method

The SWITCHCRAFT design protocol takes as input a set of multistate design constraints and produces a protein sequence that aims to satisfy those constraints. This process consists of two stages: **design specification** and **design optimization**. In specification, we construct a global constraint function that evaluates a partially-designed sequence representation $\mathbf{z} \in \mathbb{R}^{20 \times L}$ under several instantiations of Boltz-1 (Wohlwend et al., 2025), corresponding to multiple states, and returns a scalar that represents the deviation from the target design criteria. This constraint function is the sum of individual constraints that each represent a structural design criterion. In the optimization stage, we gradually refine \mathbf{z} towards a one-hot representation of a protein sequence using gradients from the global constraint function and a multi-stage optimization protocol adapted from BoltzDesign-1 (Cho et al., 2025). This framing is reminiscent of the model definition and training loop of a deep learning model; as such, we call our constraint functions *loss* functions.

Design specification A multistate design specification consists of states $s = 1, \dots, N_{\text{states}}$, each associated with a *folding context* \mathcal{C}_s , which is a (potentially empty) set of fixed molecules; a set of loss functions $\mathcal{L}_n : \mathbb{R}^{20 \times L} \rightarrow \mathbb{R}$ which expresses the desired behavior of the target sequence under the folding contexts; a design mask $\mathbf{m} \in \{0, 1\}^L$ denoting which residue positions are to be designed; and a motif sequence $\mathbf{s} \in [1, 20]^L$ for the residue identities that are not designed. Each loss depends on a subset of the states and prototypically has the functional form $\mathcal{L}_n(\mathbf{z}) = \mathcal{L}'_n(\text{Boltz-1}(\mathbf{z}, \mathcal{C}_s))$, i.e., the loss function operates over the outputs of Boltz-1, although losses that use other models or only operate on sequence properties can be conceived. Here, we define and use the following losses:

- **Motif loss.** Given a motif with residue indices $m \subset [1, L]$ and corresponding $C\beta$ positions \mathbf{r} ($C\alpha$ for glycine), we optimize for scaffolding the motif via

$$\mathcal{L}_{\text{motif}}(\mathbf{z}; m, \mathbf{r}) = \frac{1}{|m|(|m| - 1)} \sum_{i \in m} \sum_{j \neq i \in m} \sum_k p_{ijk} (d_k - \|\mathbf{r}_i - \mathbf{r}_j\|)^2 \quad (1)$$

where p_{ijk} is the distogram output of Boltz-1 for the i, j residue pair and k th bin and d_k is the midpoint distance of the k th bin. This averages the expected squared error of each pairwise distance constrained by the motif. Correspondingly, we optimize for *not* scaffolding the motif via the **anti-motif loss** $\mathcal{L}_{\text{anti-motif}} = -0.5\mathcal{L}_{\text{motif}}$.

- **Ligand loss.** Given a ligand, we optimize for binding the ligand via a loss function following BoltzDesign1 (Cho et al., 2025):

$$\mathcal{L}_{\text{ligand}}(\mathbf{z}) = \frac{1}{2c} \sum \text{mink}_j^{(k=c)} \text{mink}_i^{(k=2)} H(D_{ij} | D_{ij} < 20\text{\AA}) \quad (2)$$

where D_{ij} is the distance between the i th protein $C\beta$ position and the j th ligand and its distribution is taken from the distogram output. This maximizes the confidence of the top two contacts per ligand token for the top c tokens, where c varies from 8 to 12 over the course of the optimization. Correspondingly, we optimize for *not* binding the ligand via the **anti-ligand loss** $\mathcal{L}_{\text{anti-ligand}} = -0.5\mathcal{L}_{\text{ligand}}$.

- **Conformational change loss.** To optimize for a conformational change between two states with folding contexts $\mathcal{C}_1, \mathcal{C}_2$ we define the loss

$$\mathcal{L}_{\text{conf-change}}(\mathbf{z}; \mathcal{C}_1, \mathcal{C}_2) = -\frac{1}{L} \sum_{i=1}^L \max_{j \in [1, L]} \text{JSD}(D_{ij}^{(1)} || D_{ij}^{(2)}) \quad (3)$$

where $D_{ij}^{(1)}, D_{ij}^{(2)}$ are the distograms for residue pair i, j from the Boltz-1 outputs on folding context $\mathcal{C}_1, \mathcal{C}_2$, respectively, and JSD is the Jensen-Shannon divergence. This maximizes the distributional change for the most susceptible contact per residue index.

- **Contact loss.** Finally, to preserve that each protein state is well-predicted, we retain the intra-design contact loss from BoltzDesign1 (Cho et al., 2025):

$$\mathcal{L}_{\text{contact}}(\mathbf{z}) = \frac{1}{L} \sum_{j=1}^L \min_{i: |i-j| \geq 9} [H(D_{ij} | D_{ij} < 14\text{\AA})] \quad (4)$$

This maximizes the confidence of the top long-distance contact per residue position. We implicitly include this loss for all states in all design settings.

The global loss function is evaluated by first passing the designed sequence \mathbf{z} along with all folding contexts through Boltz-1, and summing all constituent loss terms using the cached outputs. Note that while each folding context can be thought of as a state, the molecules in each folding context are not necessarily meant to interact, as the anti-ligand loss will explicitly penalize specified interactions.

Design optimization The sequence optimization protocol randomly initializes and iteratively refines residue positions i for which $\mathbf{m}[i] = 1$, while keeping the other residue identities fixed to the motif sequence \mathbf{s} for all evaluations of the loss. At each step, the gradient of the global loss function with respect to the continuous-space sequence input \mathbf{z} is computed and used to simultaneously update all residue positions. The protocol proceeds in four stages adapted from BoltzDesign1 (Cho et al., 2025) across 240 optimization steps and terminates with a one-hot representation of the output sequence. We provide detailed pseudocode in Appendix A.1, Algorithm 1.

3 Experiments

We validate SWITCHCRAFT on six multistate design settings of increasing degrees of complexity, specified in terms of their constituent losses in Figure 1. For all settings, we run a large number of independent optimization trajectories, predict five structures with Boltz-1 for the final designed sequence in each state, and evaluate designs based on several quality criteria. Briefly, designs are checked for confident predictions based on some combination of the RMSD between the five predicted structures and/or variance of motif RMSDs. Confidence in global conformational changes is assessed via average RMSD across states versus within states (IntraRMSD). For all experiments, further details, statistics, and results can be found in Appendix B.

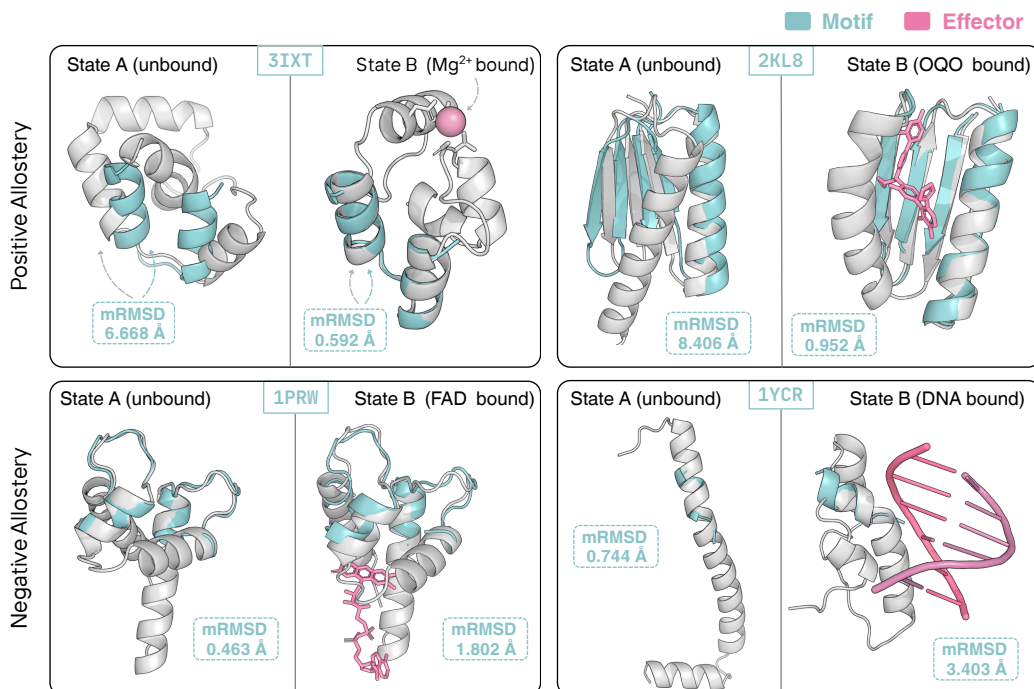


Figure 2: Selected examples of positive and negative allostery with small molecule, metal ion, and dsDNA ligands, with C α motif RMSD shown. Further analysis and statistics in Appendix B.

Positive and negative allostery. In the simplest case of multistate design, we seek to scaffold a backbone motif in the presence (absence) of a ligand in a manner such that ligand unbinding (binding) significantly disrupts the motif. For each of five ligands—small molecules OQO and flavin adenine dinucleotide (FAD); metal ions Zn²⁺ and Mg²⁺; and dsDNA with sequence GAATTC—we systematically designed scaffolds with positive and negative allostery for each of the 24 motifs from the RFDiffusion benchmark (Watson et al., 2023). We designed 100 sequences for each problem, specification, and ligand; resulting in 11 motifs having at least one success (Figure 4). Examples of successful designs visualized in Figure 2 exhibit large disruptions of the scaffolded motif, often exceeding 5 Å, associated with large conformational changes and even fold-switching of the designed protein (in the case of dsDNA). These conformational changes are confidently predicted, with low intra-state RMSDs and low variance in motif RMSDs in each state (Figures 5,6,7).

Motif switching Next, we sought to design proteins that toggle between two functional motifs upon ligand binding. Such functionality could be useful in designing dual-purpose proteins that are responsive to environmental inputs, such as pairs of enzymatic or regulatory functions. We devised a means of merging motif scaffold specifications (Algorithm 2) and constructed design specifications to toggle between motifs 3IXT and 1YCR, which exhibited the highest success rates in positive and negative allostery. Out of generated 100 designs with OQO as the effector, 3 exhibited confidently predicted scaffolding of both motifs in their respective states and disruption of each motif in the converse state (Figure 8). An example is shown Figure 3, top left and Figure 9.

Ligand modification Many natural proteins bind ligands that possess conformational or electronic properties, such as affinity for dissolved gases or light sensitivity, which are otherwise difficult to accomplish with amino acid chemistry. We sought to design proteins that could similarly leverage bound ligands to augment protein functionality. As a prototypical example, we constructed a design specification for a heme-binding protein that would exhibit a conformational change upon addition of molecular oxygen. Out of 558 designs, 10 proteins exhibited such changes (Figure 10); in our selected example, a coordinating histidine is displaced by the oxygen, inducing a 3.8 Å conformational change (Figure 3, top right; Figure 11). This conformational change is reminiscent of cooperativity in hemoglobin, which features a similar iron coordination site with two histidines. Interestingly, some examples (Figure 12) exhibited large conformational changes between the two states, but involved rearrangements that appeared implausible without unbinding and rebinding. This suggests future value in *kinetics*-based constraints to ensure plausible transitions between states.

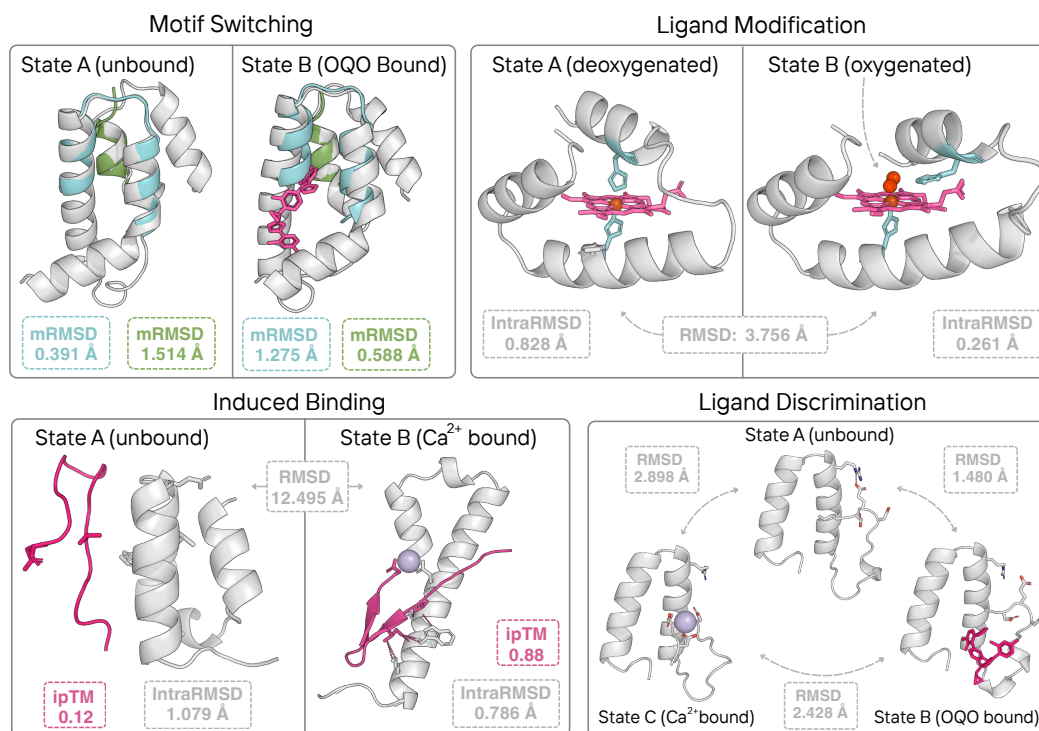


Figure 3: Case studies for motif switching, ligand modification, induced binding, and ligand discrimination design specifications. $C\alpha$ RMSDs are shown. Further analysis and results in Appendix B.

Induced binding Control over a protein’s interactions with other molecular species underlies many biological functions; for example, protein kinase A releases catalytic subunits only upon cAMP binding, and Ca^{2+} interacting with calmodulin exposes hydrophobic interfaces. We explore this class of functional control by designing proteins to engage a partner only in the presence of an effector which stabilizes or creates an interaction interface. Specifically, we sought to design a 50 AA protein that interacts with a 16 AA Top7 fragment (Kuhlman et al., 2003) in the presence of Ca^{2+} . We use ipTM as an proxy for protein-peptide binding. Out of 940 designs, 8 showed significantly higher ipTM in the presence of calcium with confidently predicted structures in both states (Figure 13). Our visualized design (Figure 3, bottom left; Figure 14) undergoes a 12.50 Å conformational change which places residues in interaction with the Top7 fragment, mediated by Ca^{2+} .

Ligand discrimination Finally, many proteins, such as enzymes with multiple intermediate states, or GPCRs with multiple signaling pathways, adopt more than two distinct ligand-dependent states. We explore the ability of our protocol to target such specifications by designing a 50-residue miniprotein to bind the ligands OQO and Ca^{2+} in separate states, each distinct from the unbound state. From 12 out of 465 successful designs (Figure 15), our visualized design possesses a key loop that adopts three distinct conformations (Figure 3, bottom right; Figure 16): forming a Glu/Arg salt bridge in the unbound state, a calcium coordination site upon calcium binding, or a hydrophobic binding pocket for OQO. The loop is confidently predicted in all three states while inducing an overall deviation of at least 1.48 Å between any two states. The successful targeting of such multi-ligand specifications hints towards the rational design of multistep enzymes with many intermediate species.

4 Conclusion

SWITCHCRAFT allows us to more broadly sample the menu of protein functions enjoyed by nature. By refining a sequence with multiple *implicit* structural constraints, we circumvent the conceptual bottleneck of prevailing single-structure design paradigms. With the additional development of constraints based on *atomic* motifs, along with creative multistate design specifications for encoding complex functions, SWITCHCRAFT is well poised to mature into a powerful framework for rational design of novel protein functions. Ultimately, we envision multistate design as a language with which we can emulate the wide and dizzying array of functions found in nature—motor proteins, rotary mechanisms, or even the information-processing polymerases that lie at the heart of biology.

References

- Woody Ahern, Jason Yim, Doug Tischer, Saman Salike, Seth M Woodbury, Donghyo Kim, Indrek Kalvet, Yakov Kipnis, Brian Coventry, Han Raut Altae-Tran, et al. Atom level enzyme active site scaffolding using rfdiffusion2. *bioRxiv*, pages 2025–04, 2025.
- Yehlin Cho, Martin Pacesa, Zhidian Zhang, Bruno E Correia, and Sergey Ovchinnikov. Boltzdesign1: Inverting all-atom structure prediction model for generalized biomolecular binder design. *bioRxiv*, pages 2025–04, 2025.
- Barry J Grant, Alemayehu A Gorfe, and J Andrew McCammon. Large conformational changes in proteins: signaling and other functions. *Current opinion in structural biology*, 20(2):142–147, 2010.
- Thomas Hayes, Roshan Rao, Halil Akin, Nicholas J Sofroniew, Deniz Oktay, Zeming Lin, Robert Verkuil, Vincent Q Tran, Jonathan Deaton, Marius Wiggert, et al. Simulating 500 million years of evolution with a language model. *Science*, 387(6736):850–858, 2025.
- Rohith Krishna, Jue Wang, Woody Ahern, Pascal Sturmfels, Preetham Venkatesh, Indrek Kalvet, Gyu Rie Lee, Felix S Morey-Burrows, Ivan Anishchenko, Ian R Humphreys, et al. Generalized biomolecular modeling and design with rosettafold all-atom. *Science*, 384(6693):ead12528, 2024.
- Brian Kuhlman, Gautam Dantas, Gregory C Ireton, Gabriele Varani, Barry L Stoddard, and David Baker. Design of a novel globular protein fold with atomic-level accuracy. *science*, 302(5649):1364–1368, 2003.
- Théophile Lambert, Amin Tavakoli, Gautham Dharuman, Jason Yang, Vignesh Bhethanabotla, Sukhvinder Kaur, Matthew Hill, Arvind Ramanathan, Anima Anandkumar, and Frances H Arnold. Sequence-based generative ai-guided design of versatile tryptophan synthases. *bioRxiv*, pages 2025–08, 2025.
- Anna Lauko, Samuel J Pellock, Kiera H Sumida, Ivan Anishchenko, David Juergens, Woody Ahern, Jihun Jeung, Alexander F Shida, Andrew Hunt, Indrek Kalvet, et al. Computational design of serine hydrolases. *Science*, 388(6744):eadu2454, 2025.
- Yeqing Lin, Minji Lee, Zhao Zhang, and Mohammed AlQuraishi. Out of many, one: Designing and scaffolding proteins at the scale of the structural universe with genie 2. *arXiv preprint arXiv:2405.15489*, 2024.
- Ali Madani, Ben Krause, Eric R Greene, Subu Subramanian, Benjamin P Mohr, James M Holton, Jose Luis Olmos Jr, Caiming Xiong, Zachary Z Sun, Richard Socher, et al. Large language models generate functional protein sequences across diverse families. *Nature biotechnology*, 41(8):1099–1106, 2023.
- Martin Pacesa, Lennart Nickel, Christian Schellhaas, Joseph Schmidt, Ekaterina Pyatova, Lucas Kissling, Patrick Barendse, Jagrity Choudhury, Srajan Kapoor, Ana Alcaraz-Serna, et al. One-shot design of functional protein binders with bindcraft. *Nature*, pages 1–10, 2025.
- Jeffrey A Ruffolo, Stephen Nayfach, Joseph Gallagher, Aadyot Bhatnagar, Joel Beazer, Riffat Hussain, Jordan Russ, Jennifer Yip, Emily Hill, Martin Pacesa, et al. Design of highly functional genome editors by modelling crispr–cas sequences. *Nature*, pages 1–8, 2025.
- Jue Wang, Sidney Lianza, David Juergens, Doug Tischer, Joseph L Watson, Karla M Castro, Robert Ragotte, Amijai Saragovi, Lukas F Milles, Minkyung Baek, et al. Scaffolding protein functional sites using deep learning. *Science*, 377(6604):387–394, 2022.
- Joseph L Watson, David Juergens, Nathaniel R Bennett, Brian L Trippe, Jason Yim, Helen E Eisenach, Woody Ahern, Andrew J Borst, Robert J Ragotte, Lukas F Milles, et al. De novo design of protein structure and function with rfdiffusion. *Nature*, 620(7976):1089–1100, 2023.
- Jeremy Wohlwend, Gabriele Corso, Saro Passaro, Noah Getz, Mateo Reveiz, Ken Leidal, Wojtek Swiderski, Liam Atkinson, Tally Portnoi, Itamar Chinn, et al. Boltz-1 democratizing biomolecular interaction modeling. *BioRxiv*, pages 2024–11, 2025.

A Additional Method Details

A.1 Design optimization

To design a sequence for a given design specification, we iteratively evaluate the loss and use its gradients to update the sequence representation. A single step of sequence optimization is shown in Algorithm 1. Note that if a motif mask is present, the motif residue types would be placed in $\mathbf{z}_{\text{pseudo}}$ as one-hot encodings before the forward pass of Boltz-1. The overall optimization protocol initializes \mathbf{z} from a Gumbel-softmax distribution and proceeds in four stages:

1. 30 steps with $\alpha = 0.2$, $\beta = 0$, $\gamma = 1$, and $\tau = 0.5$, followed by $\mathbf{z} \leftarrow \mathbf{z}_{\text{pseudo}}$
2. 100 steps with $\alpha = 0.1$, $\beta = 0$, γ interpolating from 0 to 1, and $\tau = 0.5$, followed by $\mathbf{z} \leftarrow 2\mathbf{z}$
3. 100 steps with $\alpha = 0.1$, $\beta = 0$, $\gamma = 1$, and τ interpolating from 0.5 to 0.005
4. 10 steps with $\alpha = 0.1$, $\beta = 1$, $\gamma = 1$, and $\tau = 0.005$

After optimization, we take the argmax of all non-motif residue positions.

Algorithm 1 Single step sequence optimization

```
 $\mathbf{z}_{\text{soft}} \leftarrow \text{softmax}(\mathbf{z}/\tau)$   
 $\mathbf{z}_{\text{hard}} \leftarrow \text{onehot}(\text{argmax}(\mathbf{z}'))$   
 $\mathbf{z}_{\text{hard}} \leftarrow (\mathbf{z}_{\text{hard}} - \mathbf{z}_{\text{soft}}).\text{detach}() + \mathbf{z}_{\text{soft}}$   
 $\mathbf{z}_{\text{pseudo}} \leftarrow \beta\mathbf{z}_{\text{hard}} + (1 - \beta)\gamma\mathbf{z}_{\text{soft}} + (1 - \beta)(1 - \gamma)\mathbf{z}$   
 $\mathbf{z} \leftarrow \mathbf{z} - \alpha\nabla_{\mathbf{z}}\mathcal{L}(\text{Boltz-1}(\mathbf{z}_{\text{pseudo}}))$ 
```

A.2 Motif specifications

For each of the 24 RFDiffusion (Watson et al., 2023) motifs, we follow the same protocol of sampling motif specifications from (Lin et al., 2024). Each motif specification consists of (1) an ordered list of segments, where each segment is either a *motif segment*, which is a contiguous set of motif residues, or a *scaffold segment*, which is described by a maximum and minimum length, and (2) a minimum and maximum global length. This specification allows us to generate multiple valid design problems by randomly sampling lengths of scaffold segments within their allowable ranges while preserving the global length constraints and the ordering of the motif. We use the Genie2 (Lin et al., 2024) algorithm for this procedure.

When scaffolding proteins that must accommodate *multiple* motif specifications simultaneously, we first merge them into a single unified motif specification. This merged specification can then be sampled using the Genie2 algorithm in the same way as a single-motif design. The merging procedure is outlined in Algorithm 2.

Algorithm 2 Motif Spec Merging

```
Input: Motif specifications  $M_1, M_2, \dots, M_k$   
Initialize  $S \leftarrow M_1$   
for  $i = 2$  to  $k$  do  
  Let  $T \leftarrow$  last scaffold segment of  $S$   
  Let  $L \leftarrow$  first scaffold segment of  $M_i$   
  Compute new scaffold segment to merge  $S$  and  $M_i$ :  
     $\text{min\_len} \leftarrow \max(T.\text{min\_length}, L.\text{min\_length})$   
     $\text{max\_len} \leftarrow \min(T.\text{max\_length}, L.\text{max\_length})$   
    If  $\text{min\_len} > \text{max\_len}$  then set  $\text{max\_len} \leftarrow \max(T.\text{max\_length}, L.\text{max\_length})$   
    Define new scaffold segment  $\text{Pad} \leftarrow \{\text{type}=\text{scaffold}, \text{min\_length}, \text{max\_length}\}$   
  Concatenate segments:  
     $S.\text{segments} \leftarrow S.\text{segments}[: -1] \parallel \text{Pad} \parallel M_i.\text{segments}[1 :]$   
  Recompute global min/max total lengths  
end for  
return merged motif specification  $S$ 
```

B Additional Results

B.1 Positive and negative allostery

For systematic analysis of SWITCHCRAFT’s positive/negative allostery capabilities, we designed sequence scaffolds for each of the 24 motifs from the RFDiffusion benchmark (Watson et al., 2023) across 5 ligands—small molecules OQO and flavin adenine dinucleotide (FAD); metal ions Zn^{2+} and Mg^{2+} ; and dsDNA with sequence GAATTC. We generated 100 sequences for each motif problem, specification, and ligand, resulting in 11 motifs with at least one success (Figures 4).

To quantify success, we applied the following filtering criteria. Each design yields 5 diffusion sampled structures per state (in this case two: A/B).

- **Positive allostery** (ligand promotes motif functionality): designs were required to have average motifRMSD $> 1.0 \text{ \AA}$ in the unbound state A (improperly scaffolded) and $\leq 1.0 \text{ \AA}$ in the bound state B.
- **Negative allostery** (ligand disrupts motif functionality): the inverse criteria was applied, with unbound motifRMSD $\leq 1.0 \text{ \AA}$ and bound motifRMSD $> 1.0 \text{ \AA}$.
- In both cases, we additionally required (i) motifRMSD standard deviation $\leq 0.5 \text{ \AA}$ in each state to ensure the motif scaffolding/disruption was confidently predicted, and (ii) an absolute difference in mean motifRMSD between states $\geq 0.5 \text{ \AA}$ to confirm a significant structural change.

Corresponding heatmaps of all 100 designs per motif and effector are visualized in Figure 4. Full scatterplots highlighting the bound vs. unbound average and standard deviation of motifRMSD are shown in Figures 5 and 6, with successful designs (according to the criteria above) colored pink. Example structures visualized in main text Figure 2.

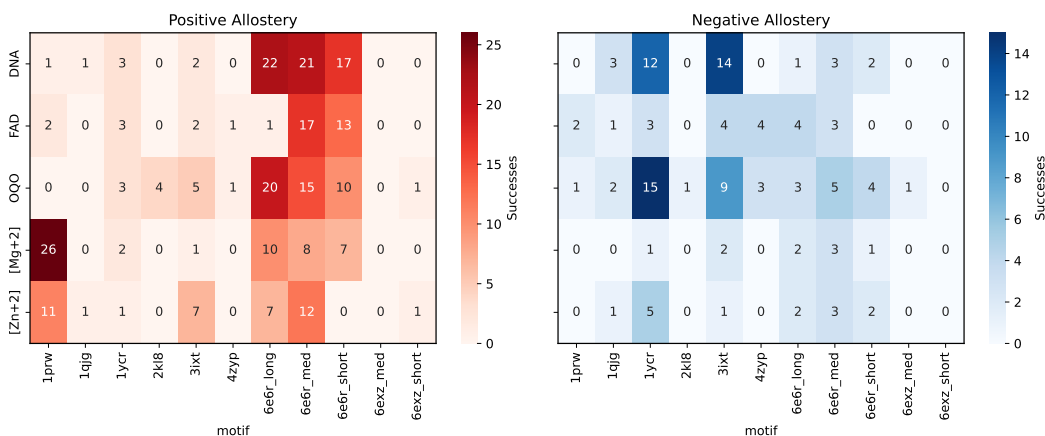


Figure 4: Success rates, out of 100 designs, for positive and negative allostery

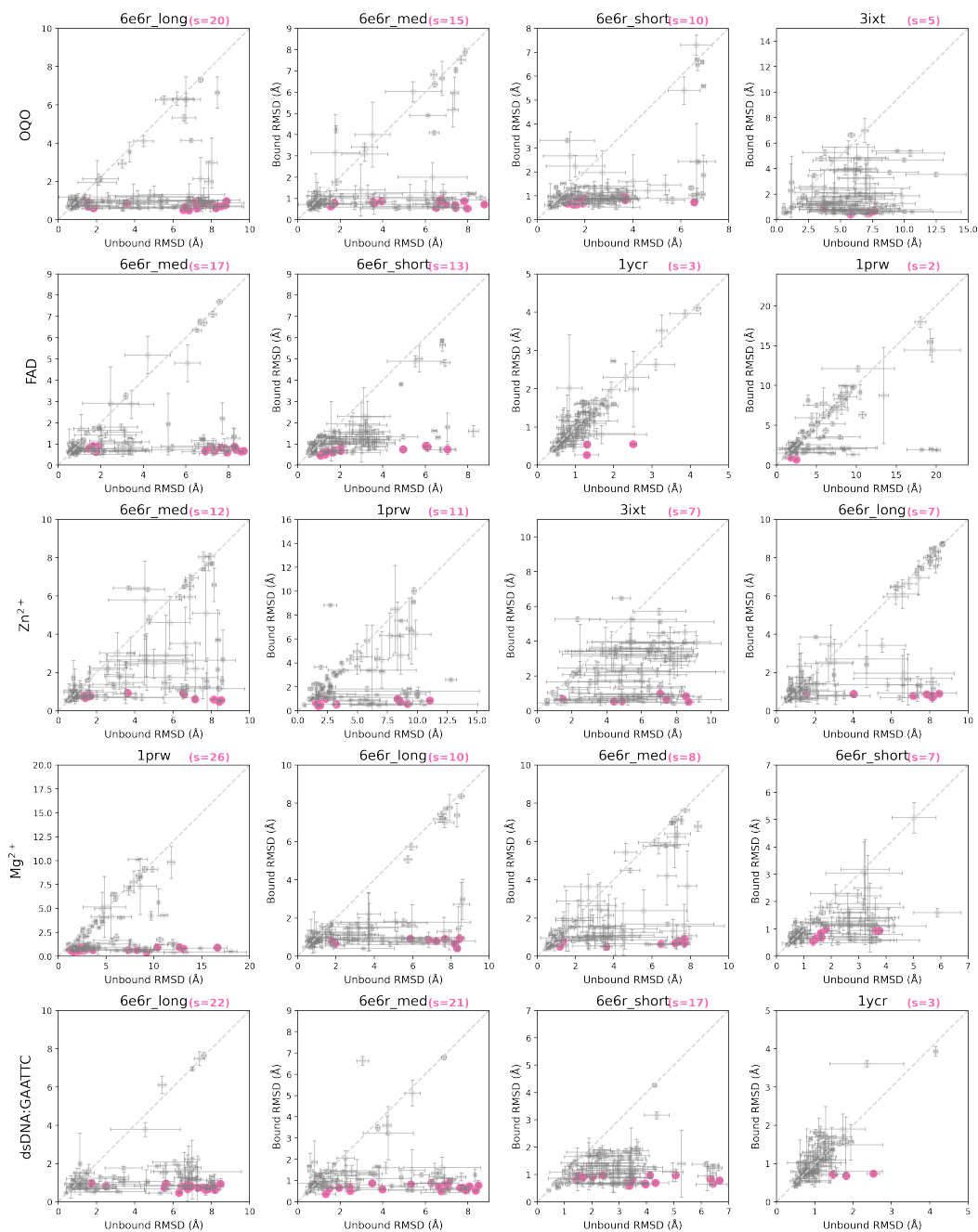


Figure 5: Positive allostery per effector/motif (top 4 success) scatter plots visualizing bound (state B) vs unbound (state A) average motif RMSD. Error bars for each design quantify motif RMSD std. Successful designs colored in pink (corresponds to Fig 4 left).

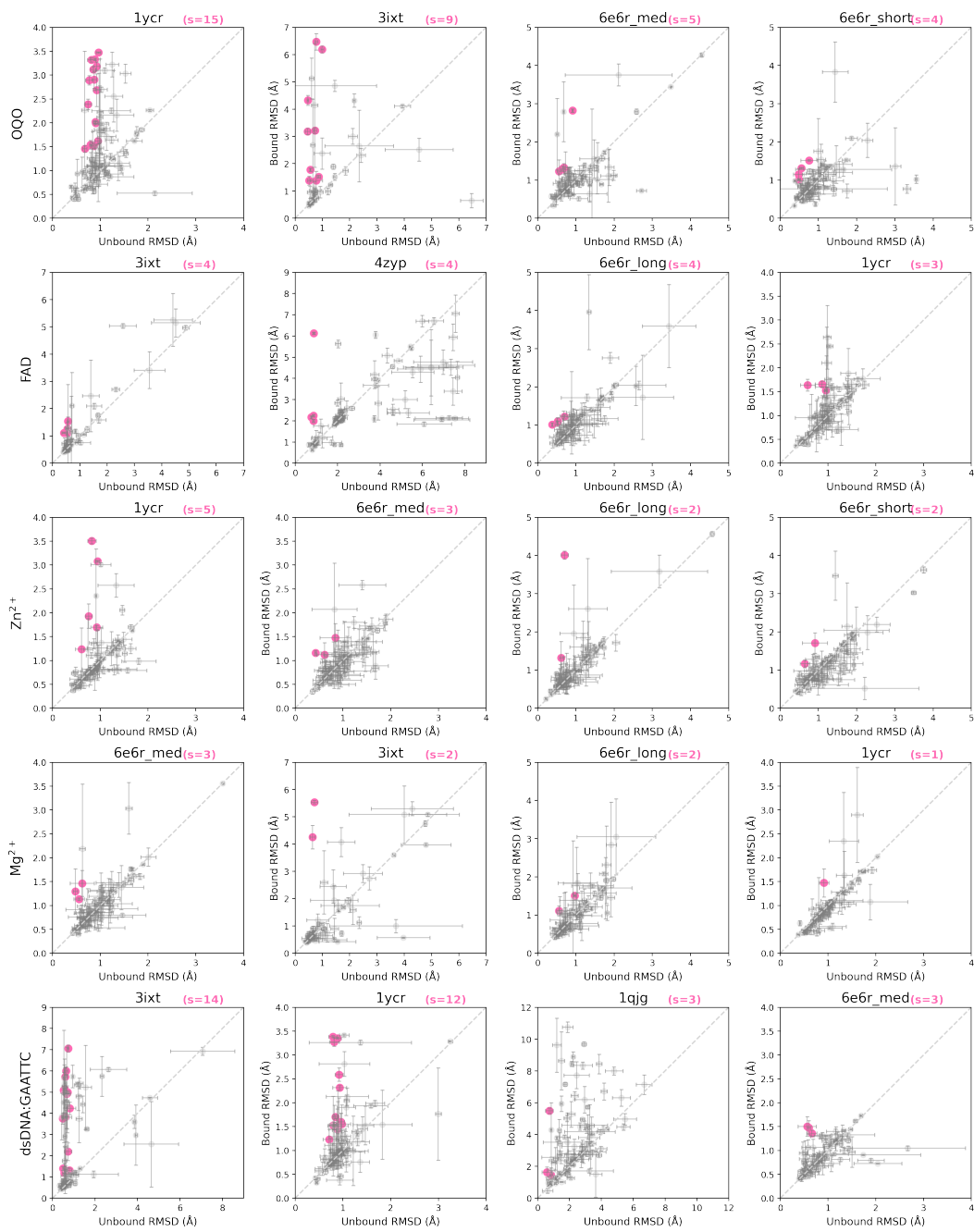
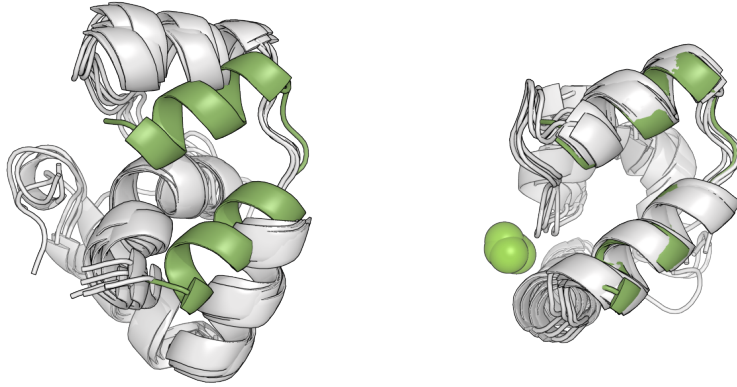
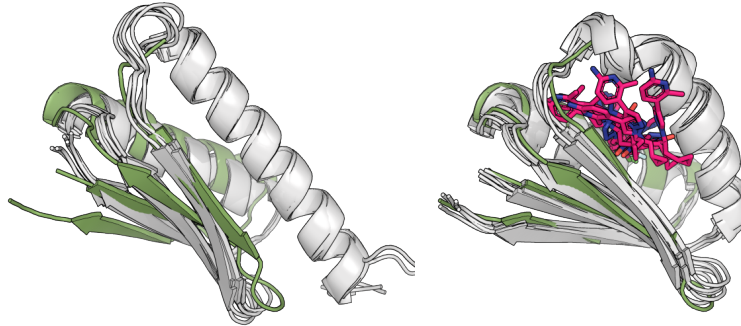


Figure 6: Negative allostery per effector/motif (top 4 success) scatter plots visualizing bound (state B) vs unbound (state A) average motif RMSD. Error bars for each design quantify motif RMSD std. Successful designs colored in pink (corresponds to Fig 4 right).

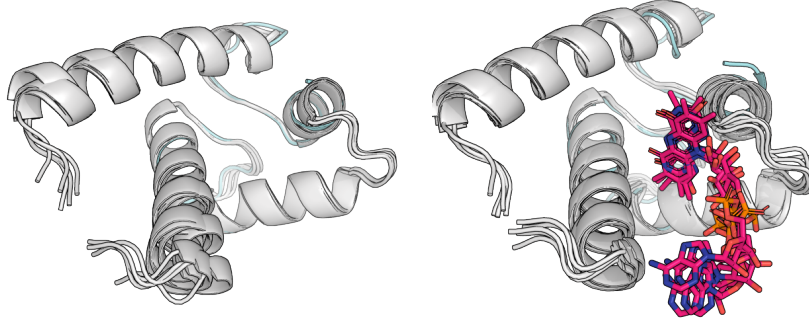
Positive allostery of 3IXT with Mg^{2+} . 3.06 Å / 1.09 Å / 8.22 Å.



Positive allostery of 2KL8 with OQO. 1.90 Å / 1.27 Å / 9.52 Å.



Negative allostery of 1PRW with FAD. 0.60 Å / 0.68 Å / 1.78 Å.



Negative allostery of 1YCR with dsDNA. 4.40 Å / 1.96 Å / 17.04 Å.

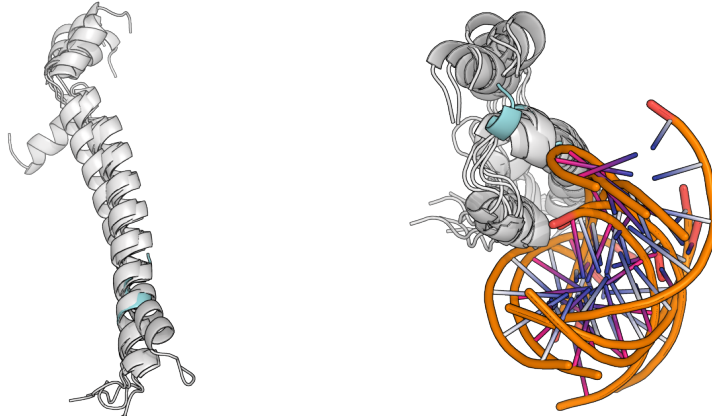


Figure 7: All predicted structures (5 each) for the positive and negative allostery designs highlighted in Figure 2. Intra-state RMSDs for the two states and cross-state $C\alpha$ RMSDs are shown.

B.2 Motif switching

We designed a scaffold containing two functional motifs, 3IXT and 1YCR, and generated 100 designs with the objective of reciprocal motif activity. Specifically, in the unbound state, the scaffold should present 3IXT in an active conformation while rendering 1YCR inactive, whereas in the OQO-bound state, the roles are reversed (1YCR active, 3IXT inactive). Thus, the following success criteria was used:

- In state A (unbound): 3IXT mean mRMSD ≤ 1.0 Å and 1YCR mean mRMSD > 1.0 Å.
- In state B (OQO-bound): 1YCR mean mRMSD ≤ 1.0 Å and 3IXT mean mRMSD > 1.0 Å.
- Additionally, mRMSD standard deviation ≤ 0.5 Å for structure confidence.

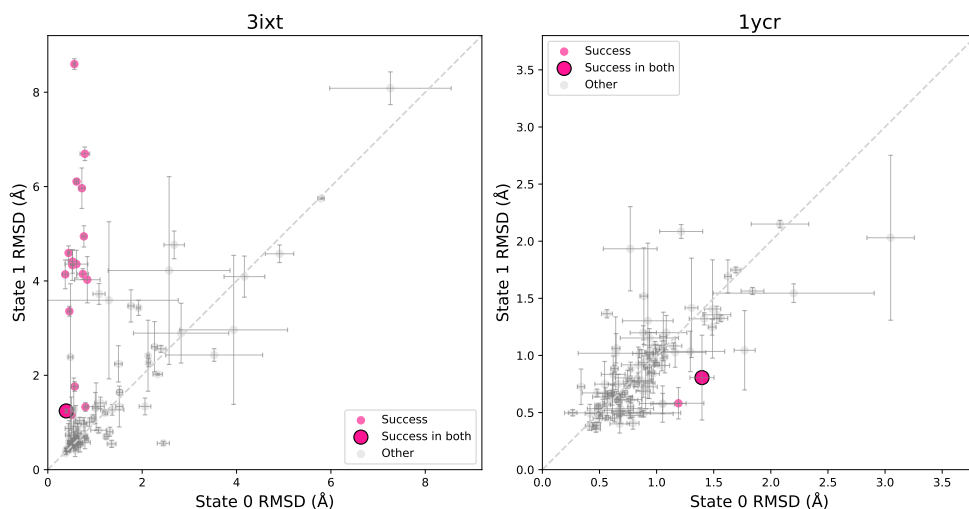


Figure 8: State B vs. State A mRMSD for each of the 100 3IXT/1YCR motif switching designs.

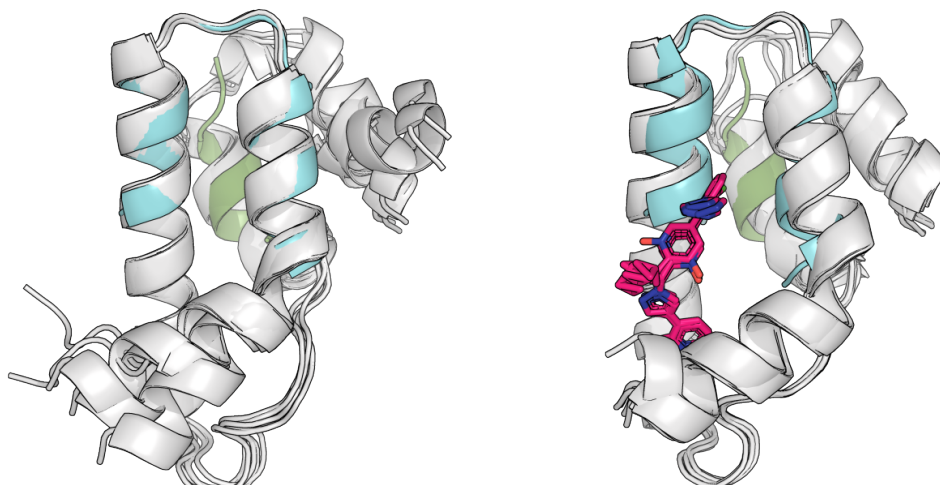


Figure 9: Predicted structures for the motif switching design. The **unbound** state A (*left*) has pLDDT=0.69, pTM=0.60, RMSD 1.93 ± 0.74 Å between samples, motif RMSD 0.39 ± 0.02 Å for 3IXT (blue), and motif RMSD 1.40 ± 0.09 Å for 1YCR (green). The **bound** state B (*right*) has pLDDT=0.79, pTM=0.80, RMSD 0.68 ± 0.38 Å between samples, motif RMSD 1.24 ± 0.04 Å for 3IXT (blue), and motif RMSD 0.68 ± 0.38 Å for 1YCR (green). The RMSD between states is 2.54 ± 0.58 Å. All RMSDs are computed for C α positions after alignment.

B.3 Ligand modification

In the ligand modification task, we sought to design a protein with two states that differ only in the chemical form of their ligand. Specifically, in state A the protein binds heme, while in state B the heme ligand is oxygenated. The design goal was to capture distinct conformational changes upon ligand modification while maintaining stability within each state. A design was considered successful if it satisfied the following criteria:

- **Intra-state stability:** intra-state RMSD $< 1.0 \text{ \AA}$ in the heme-bound state (A) or in the oxygenated-heme state (B).
- **Inter-state separation:** cross-state RMSD $> 2.0 \text{ \AA}$ between states A and B (ensuring conformational distinction).

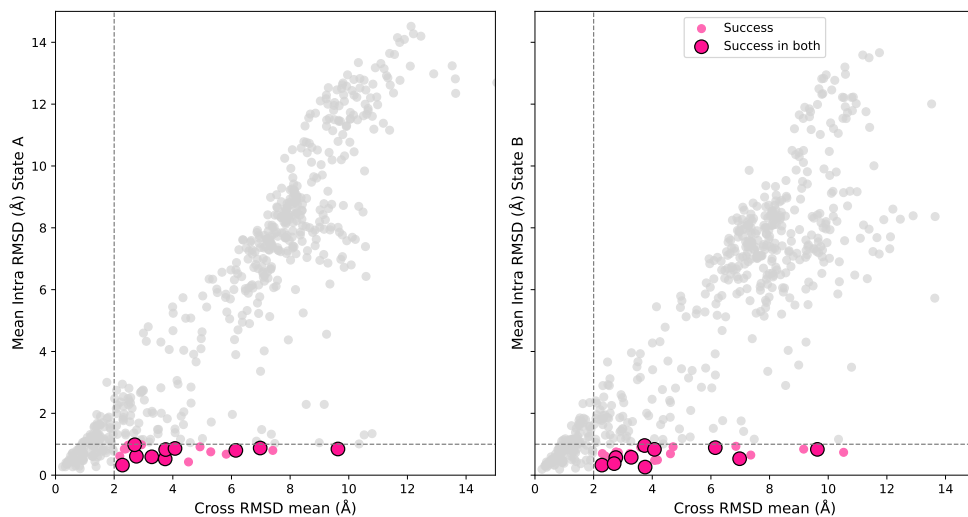


Figure 10: Success criteria for ligand modification designs. Each scatterplot shows cross-state RMSD (x-axis) versus intra-state RMSD (y-axis) for the heme-bound state A (*left*) and oxygenated-heme state B (*right*). Pink points indicate successful designs, with dark outlines denoting those that pass criteria in both states.

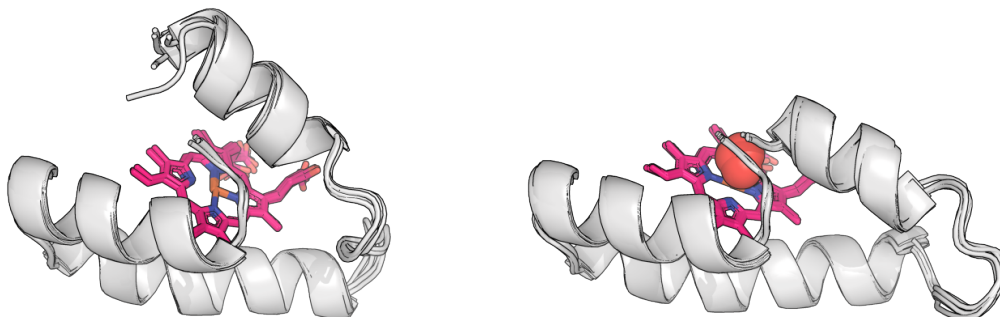


Figure 11: Predicted structures for the heme ligand modification design. The **unoxygenated** state A (*left*) has pLDDT=0.81, pTM=0.80, and RMSD $0.83 \pm 0.39 \text{ \AA}$ between samples. The **oxygenated** state B (*right*) has pLDDT=0.91, pTM=0.94, and RMSD $0.26 \pm 0.05 \text{ \AA}$ between samples. The RMSD between states is $3.76 \pm 0.08 \text{ \AA}$. All RMSDs are computed for $C\alpha$ positions after alignment.

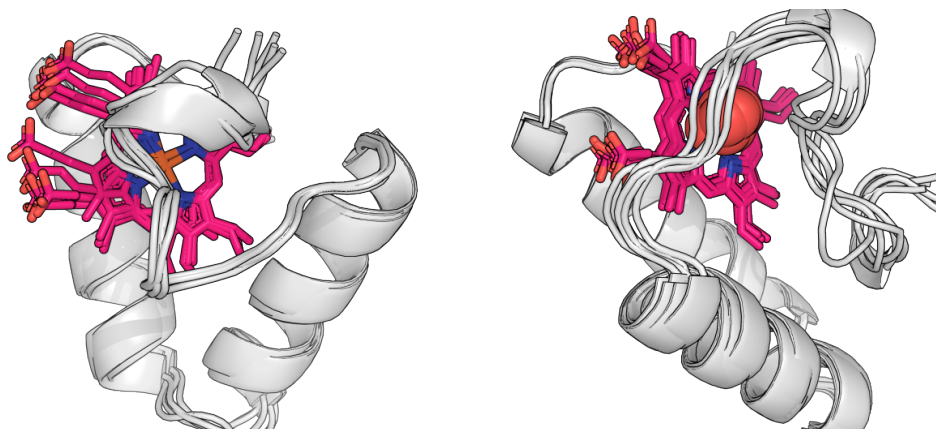


Figure 12: An alternative ligand modification design with a large but kinetically implausible conformational change. The **unoxygenated** state A (*left*) has pLDDT=0.74, pTM=0.68, and RMSD 0.85 ± 0.18 Å between samples. The **oxygenated** state B (*right*) has pLDDT=0.77, pTM=0.82, and RMSD 0.83 ± 0.31 Å between samples. The RMSD between states is 9.63 ± 0.18 Å.

B.4 Induced binding

For the induced binding task, we wanted to design a protein that binds a Top7 fragment only in the presence of calcium, while remaining unbound in the calcium-free state. A design was considered successful if it satisfied the following conditions:

- **Binding specificity:** ipTM < 0.6 in the unbound state (no binding) and ipTM > 0.6 in the calcium-bound state (binding).
- **Conformational change:** inter-state RMSD > 3.0 Å between bound and unbound states.
- **Structural confidence:** intra-state RMSD < 2.0 Å within each state ensemble.

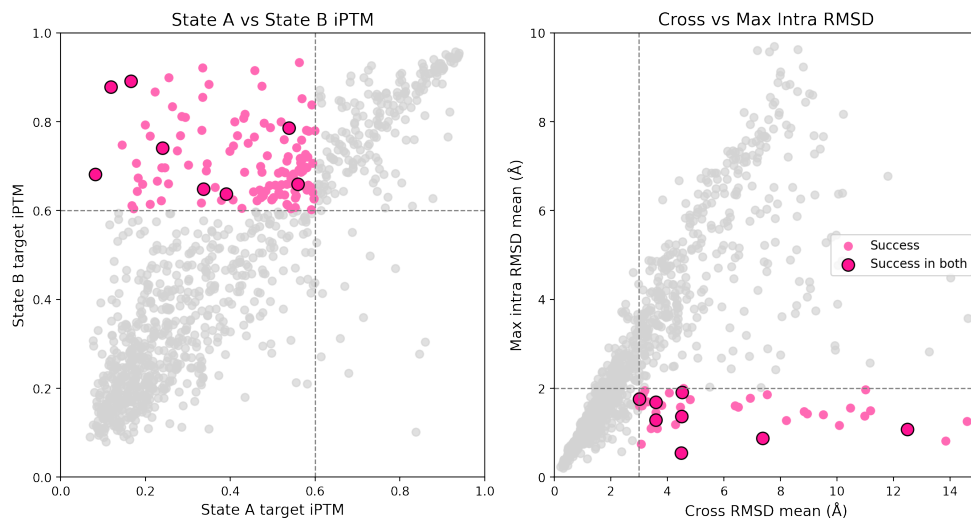


Figure 13: Success criteria for induced binding designs. **(Left)** ipTM in the unbound (state A) versus calcium-bound (state B) **(Right)** Cross-state versus intra-state RMSD. Pink points indicate designs meeting success thresholds, with dark outlines denoting designs that pass both sets of criteria.

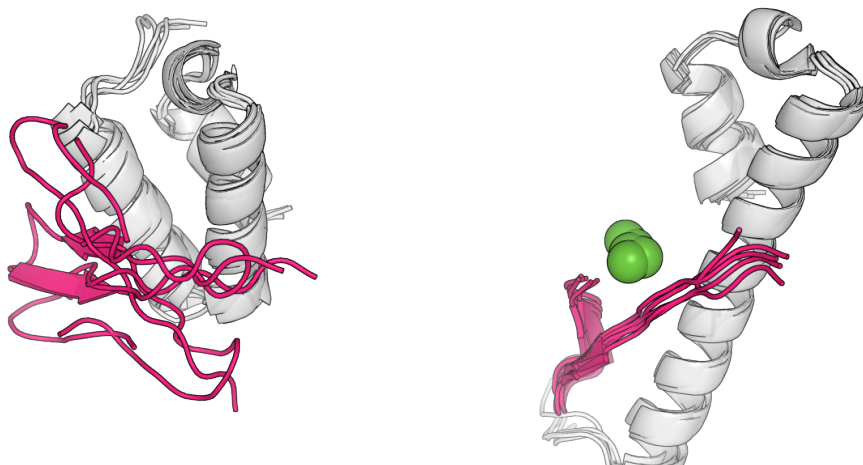


Figure 14: Predicted structures for the induced binding design. The **unbound** state A (*left*) has pLDDT=0.57, pTM=0.49, ipTM 0.12, and RMSD 1.08 ± 0.22 Å between samples. The **bound** state B (*right*) has pLDDT=0.85, pTM=0.80, ipTM 0.88 with respect to the target peptide, ipTM 0.62 with respect to the calcium effector, and RMSD 0.79 ± 0.14 Å between samples. The RMSD between states is 12.50 ± 0.17 Å. All RMSDs are computed for C α positions of the design after alignment.

B.5 Ligand discrimination

In the ligand discrimination task, we sought to design a protein with three distinct conformational states: (A) the **unbound** state, (B) the **OQO-bound** state, and (C) the **calcium-bound** state. Each state should be structurally stable on its own, while differing substantially from the other states to reflect distinct ligand-specific conformations. The success criterion is as follows,

- **Intra-state stability:** intra-state RMSD $< 1.0 \text{ \AA}$ for all three states (ensuring consistent conformations within each ensemble).
- **Inter-state separation:** pairwise cross-state RMSD $> 1.0 \text{ \AA}$ for all three pairs of states (ensuring distinct conformations between states).

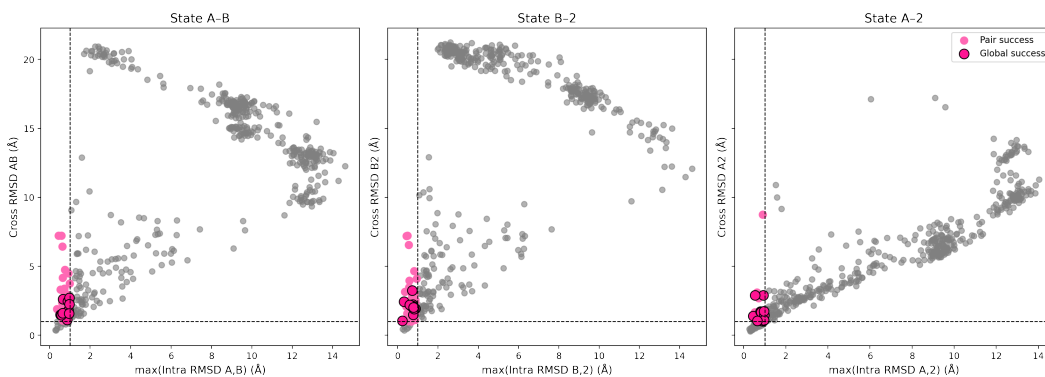


Figure 15: Success criteria for ligand discrimination designs. Each scatterplot shows the cross-state RMSD between a pair of states versus the maximum intra-state RMSD (where higher values indicate less consistency). Pink points indicate pairwise or global successes (outlined).

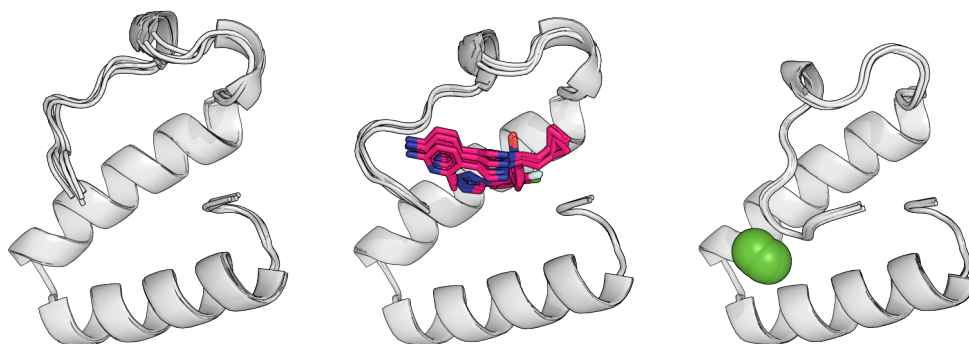


Figure 16: Predicted structures for the ligand discrimination design. The **unbound** state A (*left*) has pLDDT=0.75, pTM=0.56, and RMSD $0.53 \pm 0.13 \text{ \AA}$ between samples. The **OQO-bound** state B (*center*) has pLDDT=0.85, pTM=0.90, and RMSD $0.31 \pm 0.04 \text{ \AA}$ between samples. The **calcium-bound** state C (*right*) has pLDDT=0.86, pTM=0.89, and RMSD $0.21 \pm 0.03 \text{ \AA}$ between samples. The RMSD between states is A/B: $1.48 \pm 0.13 \text{ \AA}$; A/C: $2.90 \pm 0.10 \text{ \AA}$; B/C: $2.42 \pm 0.09 \text{ \AA}$. All RMSDs are computed for $C\alpha$ positions of the design after alignment.